https://doi.org/10.1016/j.jsv.2020.115266

Partition of Unity Finite Element Method for the modeling of Acoustic Black Hole Wedges

T. Zhou[a], J.-D. Chazot[b], E. Perrey-Debain[b], L. Cheng[a,*]

[a]*Department of Mechanical Engineering, The Hong Kong Polytechnic University, Hong Kong, P. R. China*
[b]*Laboratoire Roberval, FRE UTC-CNRS 2012, Université de Technologie de Compiègne, 60205 Compiègne, BP 20529, France*

Abstract

The Acoustic Black Hole (ABH) phenomenon can be exploited to manipulate and mitigate flexural wave propagation in thin-walled structures. ABH structures feature unique space-dependent wavenumber variation and wave celerity reduction in the tapered ABH area, thus posing challenges to the existing modelling techniques. In this work, the Partition of Unity Finite Element Method (PUFEM) is revamped to simulate the structural response of an ABH wedge subject to a harmonic loading. This method allows the incorporation of auxiliary enrichment functions into the finite element framework in order to cope with the ABH-induced wave oscillating behaviour, exemplified by the varying wavenumber and amplitude in space. The PUFEM tapered Timoshenko beam elements are constructed by employing wave enrichment functions with the Wentzel-Kramers-Brillouin (WKB) approximation method. A wavelet enrichment is also investigated as hierarchic refinement. Using these enriched elements, the frequency responses of an ABH wedge and the convergence of numerical solutions are computed and compared with the classical linear FEM and the elements enriched with 'local' wave solutions. An adaptive meshing scheme is designed and implemented to further accelerate the solution convergence. It is shown that the PUFEM offers a good computational accuracy and drastic reduction of degrees of freedom for solving the broadband ABH problems, outperforming the classical FEM.

Keywords: Acoustic Black Hole, Partition of Unity Finite Element Method, WKB method, Wavelet
PACS:

1. Introduction

The Acoustic Black Hole (ABH) phenomenon shows good prospects for the manipulation and mitigation of the flexural bending waves in mechanical structures like beams and plates. An ABH-featured structure is tailored with a smoothly decreasing thickness profile according to a power-law function $h(x) = cx^{\nu}$, where $\nu \geq 2$ and c is a constant [1]. As the flexural waves travel towards the thin ABH section, the incident wave undulates with a continuous increase of wavenumbers and a gradual reduction of wave celerity, alongside an amplification of the wave amplitude. In an ideal scenario where the thickness goes to zero, waves would spend infinitely long time to travel inside the ABH area, thus resulting in no wave reflections. Meanwhile, the vibrational energy is focused and accumulated in the thin tapered region due to the wave

*Corresponding authors
Email address: li.cheng@polyu.edu.hk (L. Cheng)

modulations and compression induced by the structural inhomogeneity. In practical cases where the zero thickness is non-achievable, applying surface damping treatment over the tapered region can significantly reduce the wave reflections and enhance the energy absorption [2].

Various models have been exploited to characterize the ABH phenomena. The Wentzel-Kramers-Brillouin (WKB) method was first used to analyse the dispersion properties of flexural wave propagation in a tapered wedge [1]. Preliminary ABH studies based on the WKB approach mainly focused on the wavenumber analysis of the travelling waves in a semi-infinite wedge-like beam [1, 2]. Other models, not limited by the sufficient smoothness hypothesis of the WKB approach, were also used to deal with ABH structures with more realistic geometrical configurations and boundary conditions. Typical examples include finite difference approaches [3], impedance matrix methods [4], transfer matrix methods [5], wavelet-decomposed Rayleigh-Ritz models [6] and Finite Element Method (FEM) [7, 8] etc. ABH-profiled structures feature unique space-dependent wavenumber variation and wave celerity reduction over a broad frequency range. Therefore, most methods require a refined discretization scheme with high resolution in order to capture the strongly localized and highly oscillatory ABH behaviours, especially when the local wavelengths in ABH cells become shorter. For example, a dense mesh grid should be adopted by the finite difference method [3] and conventional FEM [8], while the wavelet series with refined scales or short support length should be chosen as the global expansion functions in Rayleigh-Ritz methods [6]. This, inevitably, leads to a drastic increase in the computational cost, which may become crucial when dealing with more complicated ABH problems such as structures with multiple embedded ABH cells or auxiliary ABH absorbers [9, 10], parameter optimizations of ABH tapers [11, 12], interactions of ABH structures with surrounding medium, and so on. Therefore, there is a need to develop more efficient simulation tools capable of better capturing the shortened local wavelengths as well as the amplified oscillating behaviours along the ABH taper in a broad frequency band.

In recent decades, enriched numerical methods have been developed to improve the computational efficiency and accuracy for the short-wave modeling, which usually involves a large number of wavelengths in the problem domain. These simulation techniques allow the incorporation of auxiliary functions with good approximation properties for the concerned problems in the formulation stage. As one of these enriched methods, the Partition of Unity Finite Element Method (PUFEM) [13, 14] offers the advantage of sharing high similarities with the conventional FEM, thus allowing easy implementation by using existing finite element meshes and codes. The PUFEM has been applied to acoustic and elastic wave propagation problems in homogeneous media with a uniform wave speed [15, 16, 17, 18]. It has been shown that the enriched elements can achieve accurate predictions with a significant reduction of the degrees of freedom in comparison with the conventional FEM. Applications of the PUFEM to problems with location-dependent wave celerity or wavenumber are mainly limited to acoustic problems up to now. Typically, Lagrange multipliers were used to enforce the element continuity between domains with an abrupt jump of sound speed [19, 20, 21]. Special short-wave elements are constructed for modelling acoustic and water wave propagation in media with continuous variations of wave speeds in space [22, 23, 24, 25, 26]. The local wave solutions for the equation of motion in the vicinity of a node (or plane-wave basis) are chosen as the auxiliary enrichment functions [22, 24]. These elements are mainly applicable for cases where the change in wavenumbers within a single element is not significant.

In this work, the PUFEM is adapted to simulate the structural vibrations of a wedge-like ABH beam. Different formulations are proposed to deal with the broadband ABH-specific problems, aiming at improving the computational accuracy and efficiency of the PUFEM. The tapered Timoshenko beam elements are first constructed by using wave enrichment functions with

the WKB approximation method. These enriched elements are crafted with the information of solutions obtained from the governing differential equations of the tapered beam. Wavelet functions, which possess localized compact support properties conducive to representing the ABH oscillations, are also taken as the enrichment functions of the PUFEM. Comparisons are made with the element enriched with the 'local' wave solutions for the tapered beams as well as the classical linear FEM. The performance of these elements is evaluated in terms of computational accuracy and data reduction. Numerical analyses are carried out on a quadratic ABH wedge, so the applicability of the WKB-based enrichment can be checked against the enrichment using analytical wave solutions, which only exist for a quadratic wedge.

The outline of the paper is as follows. In section 2, after recalling the basic theory of the tapered beam vibration, the WKB wave solutions by the Euler-Bernoulli and Timoshenko beam models are given and these wave functions are to be employed to build the PUFEM Timoshenko beam elements. Formulations of the element enriched with wavelet functions and the other enriched elements are also presented in this section. In section 3, the performance of different PUFEM elements and that of the classical linear FEM is shown and compared. Convergence curves, obtained using the mesh refinement by reducing the uniform element length or the hierarchic refinement by increasing the wavelet scaling parameters, are presented and analyzed. An adaptive mesh scheme is proposed to further reduce the calculation errors and enhance the solution convergence. The applicability of the WKB approximate solution as enrichment functions for PUFEM is then discussed. Finally, conclusions are drawn in the last section.

2. Formulation

2.1. Statement of the problem

Consider the flexural vibration of a beam with a variable thickness $h(x)$ and a constant width t in Fig. 1 (a). We are interested in the structural response of the tapered beam subject to a harmonically oscillating loading at a circular frequency $\bar{\omega}$ so that the time-dependent term $e^{-i\bar{\omega}\bar{t}}$ is omitted hereafter ($i = \sqrt{-1}$). There are two main theories dedicated to beams: Euler-Bernoulli and Timoshenko theories. For the former, the axial displacement of the beam, at a distance z from the neutral layer, is written as $u(x, z) = -zw'$, where $w(x, z) = w(x)$ is the lateral displacement of mid-surface in z direction and the prime donates the spatial derivative with respect to the coordinate x. For the latter, the beam axial displacement is replaced by $u(x, z) = z\beta(x)$, where $\beta(x)$ is the rotation angle of the cross section. The equation of motion of a tapered Euler-Bernoulli beam is given by

$$[EI(x)w'']'' - \bar{\omega}^2\rho A(x)w - f_z = 0, \tag{1}$$

and those of a tapered Timoshenko beams write

$$[\kappa GA(x)(\beta + w')]' + \bar{\omega}^2\rho A(x)w + f_z = 0, \tag{2}$$

$$\kappa GA(x)(\beta + w') - [EI(x)\beta']' - \bar{\omega}^2\rho I(x)\beta = 0, \tag{3}$$

where f_z is the distributed oscillating loading. For a transverse point force located at $x = x_f$ on the beam, the loading term can be expressed as $f_z = F_0\bar{\delta}(x - x_f)$, where $\bar{\delta}(\cdot)$ is the Dirac delta function. Geometrical parameters involved in the above equations are the area moment of inertia $I(x) = t\,h^3(x)/12$, the cross section area $A(x) = t\,h(x)$ and the shear correction factor $\kappa = 5/6$ for a rectangular cross-sectional beam [27]. Material parameters are the Young's modulus E, the shear modulus G and the density ρ. The Euler-Bernoulli beam model, as a special case of a Timoshenko beam, neglects the effects of the shear deformation and rotary

inertia. This simplified model is widely used in the existing literature on various aspects of ABH phenomena.

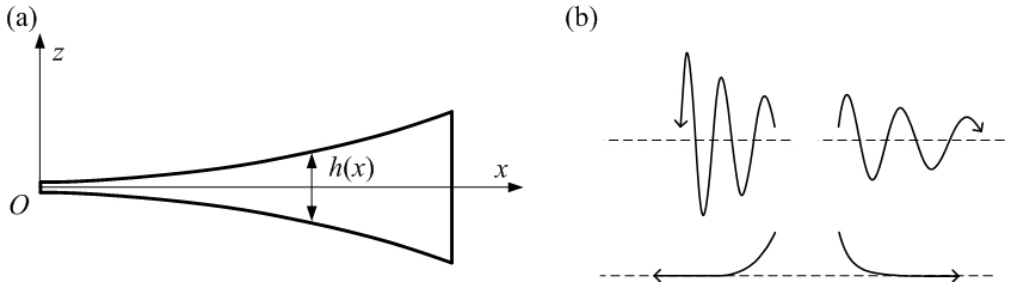

Figure 1: (a) Schematics of the ABH wedge and (b) four possible free waves associated with one node.

2.2. Wave solutions

The closed-form solutions for Eq. (1) or Eqs. (2) and (3) in terms of elementary functions are difficult to be found, so that we have to resort to using approximate solutions. The WKB method provides appropriate approximate solutions to the differential equations whose coefficients are slowly varying function in space [28, 29]. For a tapered Euler-Bernoulli beam, the WKB constant-frequency solutions to Eq. (1) can be sought as a set of four waves:

$$w_n(x) = \widehat{w}_n(x)e^{iS_n(x)},\ n = 1, 2, 3, 4, \tag{4}$$

where $S_n(x)$ is the eikonal of the quasi-plane wave (or the generalized phase) and $\widehat{w}_n(x)$ is the varying amplitude function. The spatial derivative of the eikonal $k_n(x) = S_n'$ can be solved from the so-called 'eikonal equation' [2, 29]. The expression of $k_n(x)$ writes

$$k_n(x) = (i)^n \left[\frac{\rho A(x)}{EI(x)}\bar{\omega}^2\right]^{1/4}. \tag{5}$$

Here, the two real-valued solutions ($n = 2, 4$) correspond to the two oscillatory waves travelling in two opposite directions and the other two imaginary solutions ($n = 1, 3$) correspond to the near-field evanescent waves. The local wavenumber along the beam is given by $\bar{k}(x) = |k_n(x)|$. The eikonal $S_n(x)$ can be found by integrating $k_n(x)$ over space. The wave amplitude function $\widehat{w}_n(x)$ is determined from the energy-conservation theorem or the corresponding 'transport equation' as [29, 30, 31]

$$\widehat{w}_n(x) = C[\rho A(x)]^{-3/8}[EI(x)]^{-1/8}, \tag{6}$$

where C is a constant and $\widehat{w}_n(x)$ is the same for the four types of waves. The applicability of the WKB method relies on the sufficient smoothness condition of the beam thickness variation. The spatial change of the local wavenumbers should be small over a distance of wavelength order [1]. This condition yields the inequality:

$$\frac{\bar{k}'(x)}{\bar{k}^2(x)} \ll 1 \tag{7}$$

The left-hand side term of condition (7) is referred to as the 'Normalized Wavenumber Variation' (NWV) [7], which gives an estimation on the applicability range of the WKB approximation. The NWV depends on both the position along the beam and the vibration frequency.

The WKB solutions for the displacement and rotation of a tapered Timoshenko beam take the form

$$w_n(x) = \widehat{w}_n(x)e^{iS_n(x)} \ , \ \beta_n(x) = \widehat{\beta}_n(x)e^{iS_n(x)}. \tag{8}$$

The expressions of $k_n(x) = S_n'$ corresponding to the four types of waves are given by

$$k_{1,2,3,4} = \pm \left[\frac{1}{2}\left(\frac{1}{\kappa G} + \frac{1}{E}\right)\rho\bar{\omega}^2 \pm \sqrt{\frac{1}{4}\left(\frac{1}{\kappa G} - \frac{1}{E}\right)^2 \rho^2\bar{\omega}^4 + \frac{\rho A(x)}{EI(x)}\bar{\omega}^2} \right]^{1/2}. \tag{9}$$

where the index $n = 1, 2, 3, 4$ refers to one of the four combinations in (9). The displacement amplitude function is written as [29]

$$\widehat{w}_n(x) = C\left[\frac{k_n(x)}{\rho A(x)}\right]^{1/2}\left[1 + \frac{I(x)}{2A(x)}\left(\frac{E}{\kappa G} - 1\right)\left(\frac{\rho\bar{\omega}^2}{\kappa G} - k_n^2(x)\right)\right]^{-1/2}. \tag{10}$$

The amplitude function for the cross-section rotation angle can be determined by using the relation $\widehat{\beta}_n(x) = i\widehat{w}_n(x)[\rho\bar{\omega}^2/\kappa G k_n(x) - k_n(x)]$. The ABH effects can be revealed by analyzing the WKB solutions for the tapered wedge whose thickness follows $h(x) = cx^\nu$. Figure 2 depicts the dependence of the local wavenumbers and the wave celerity on the location and frequency of the propagating flexural waves in a quadratic ABH wedge ($\nu = 2$), which is calculated from the Timoshenko model.

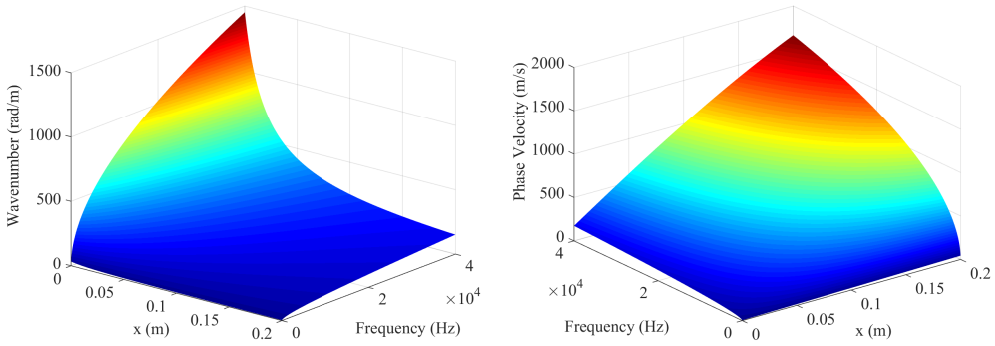

Figure 2: The wavenumber and phase velocity of propagating flexural wave in a quadratic AHB wedge (calculated using the parameters in Table 1)

For a specific Euler-Bernoulli ABH beam with a quadratic thickness variation $h(x) = cx^2$, analytical wave solutions in terms of the power functions can be derived [32]. The analytical solution to Eq. (1) is sought by

$$w(x) = Cx^{p_n}, \tag{11}$$

where

$$p_{1,2,3,4} = -\frac{3}{2} \pm \left[\frac{17}{4} \pm \sqrt{4 + 12\frac{\rho\bar{\omega}^2}{Ec^2}}\right]^{1/2}. \tag{12}$$

This analytical solution is not limited by the sufficient smoothness condition (7) and is more accurate than the corresponding WKB Euler-Bernoulli solution, especially in the low frequency range.

2.3. PUFEM tapered Timoshenko beam elements

As compared with Euler-Bernoulli beams, Timoshenko beams offer an easier platform for the implementation of the PUFEM [18]. For a free-free tapered Timoshenko beam, the associated variational formulation to Eqs. (2) and (3) writes:

$$\int_0^L \left(\bar{\omega}^2 \delta w \rho A(x) w + \bar{\omega}^2 \delta\beta \rho I(x)\beta + \delta\beta' EI(x)\beta' + (\delta\beta + \delta w')\kappa GA(x)(\beta + w') - \delta w f_z\right) \mathrm{d}x = 0, \tag{13}$$

where $\delta(\cdot)$ donates the virtual quantity and $x = 0, L$ are the positions of two beam ends. Lagrange multipliers can be used to enforce the essential boundary conditions with PUFEM and the coupling conditions between two domains with different characteristics (see for instance Refs. [19, 20, 21]).

Similar as in classical FEM, the tapered beam is discretized by a set of nodes into a number of non-overlapping elements and each node is associated with a given number of degrees of freedom (DoFs). The translational and rotational displacements within each element are expressed by a set of piecewise basis functions in terms of nodal unknowns. The key ingredient of the PUFEM relies on the choice of an appropriate enrichment for the conventional finite element approximation by including special auxiliary functions with good approximation properties for the solutions of the concerned problems. Each PUFEM beam element of length $l_e = x_2 - x_1$ is given by the geometric mapping $x(\xi) = N_1 x_1 + N_2 x_2$, where x_1 and x_2 are the nodal positions and $\xi \in [-1, 1]$ is the local coordinate. Here, $N_1 = (1 - \xi)/2$ and $N_2 = (1 + \xi)/2$ are the classical linear shape functions. In each element, the lateral displacement and rotation are expanded, respectively, as:

$$w = \sum_{m=1}^{2} N_m(\xi) \sum_n a_{m,n}\, \Phi_{m,n}, \tag{14}$$

$$\beta = \sum_{m=1}^{2} N_m(\xi) \sum_n b_{m,n}\, \Psi_{m,n}. \tag{15}$$

The computational performance of the PUFEM is dependent upon the choice of the enrichment functions $\Phi_{m,n}$ and $\Psi_{m,n}$. These functions are not necessarily the exact solutions to the governing differential equations of the tapered Timoshenko beam (see Ref. [14]). Therefore, the PUFEM allows flexible choice of enrichment. Several types of enrichment methods are tested and assessed in the following sections, aiming at improving the computational performance of the PUFEM.

For the wave enrichment, the WKB approximate solutions for tapered Euler-Bernoulli beams (Eq. (4)) and tapered Timoshenko beams (Eq. (8)) can be taken as enrichment functions $\Phi_{m,n}$ and $\Psi_{m,n}$. The Euler-Bernoulli solutions for the rotation are sought by using the relation $\beta = -w'$. The WKB wave enrichment functions write

$$\{\Phi_{m,n}\} \in \{1, \widehat{w}_1(x)e^{iS_{m,1}}, \widehat{w}_2(x)e^{iS_{m,2}}, \widehat{w}_3(x)e^{iS_{m,3}}, \widehat{w}_4(x)e^{iS_{m,4}}\}, \tag{16}$$

$$\{\Psi_{m,n}\} \in \{1, \widehat{\beta}_1(x)e^{iS_{m,1}}, \widehat{\beta}_2(x)e^{iS_{m,2}}, \widehat{\beta}_3(x)e^{iS_{m,3}}, \widehat{\beta}_4(x)e^{iS_{m,4}}\}, \tag{17}$$

where the subscript donates four possible free wave solutions associated with a node x_m (Fig. 1 (b)) and the eikonal term is defined as $S_{m,n}(x) = \int_{x_m}^{x} k_n(s)\mathrm{d}s$. The wave enrichment functions in Eqs. (16) and (17) are expressed in terms of the unmapped physical coordinate x. In addition to the four free waves, a constant term is also added to the enrichment basis in order to capture the contribution of the loading and to enhance the convergence of the numerical solutions [18].

For an ABH thickness variation $h(x) = cx^{\nu}$, the WKB Euler-Bernoulli wavenumber $\bar{k}(x)$ has a simple expression so that the analytical expression of $S_{m,n}$ can be found. The eikonal term $S_{m,n}$ of a tapered Timoshenko beam can be evaluated using numerical integration, while the WKB Timoshenko enrichment is believed to lead to better convergence at higher frequencies.

For the sake of comparisons, an enrichment based on the analytical solutions for quadratic Euler-Bernoulli wedges and an enrichment based on 'local' wave solutions for tapered Timoshenko beams are also studied. The former can be carried out in a similar manner as the WKB wave enrichment, through using the equivalent exponential expression of Eq. (11) in Ref. [32]. For the latter, the enrichment functions are given by

$$\{\Phi_{m,n}, \Psi_{m,n}\} \in \{1, e^{ik_{m,1}(x-x_m)}, e^{ik_{m,2}(x-x_m)}, e^{ik_{m,3}(x-x_m)}, e^{ik_{m,4}(x-x_m)}\}, \tag{18}$$

where $k_{m,n}$ is evaluated at the node x_m by Eq. (9). Other conventional enrichment methods for PUFEM, such as the polynomial enrichment used in Ref. [18], can also be taken for comparison purposes. The polynomial-enriched elements usually show advantages over high-order enhanced Timoshenko beam elements [18, 33]. It was also found that the local wave enrichment offers slightly better computational performance than polynomial enrichment with the same number of enrichment terms at each node. Therefore, only the results from the former are shown in the following analyses to facilitate the discussion.

The PUFEM with wavelet enrichment is then developed and investigated in this work. The wavelet functions have compact-supported or fast-decaying oscillating shapes [34, 35] and possess the superior capability to represent the solutions with strongly localized variation pattern, which is conducive to capturing the ABH-induced wave compression phenomenon [6, 36]. The spline scaling functions [34, 35, 37] used in the wavelet analysis are chosen as the enrichment functions:

$$\{\Phi_{m,n}, \Psi_{m,n}\} \in \{1, \ldots, 2^{j/2}\varphi_r(2^j\eta_m - n), \ldots, \text{ for } n \in \mathbb{Z}\}, \tag{19}$$

where $\eta_m = (x - x_m)/l_e$, φ_r is cardinal B-spline function of order r, $j \in \mathbb{Z}$ is the scaling parameter and n is the translation parameter. The constant term is added to the above PUFEM basis to ensure a good approximation of the solution in the present case. In addition, it is also helpful when imposing essential boundary conditions of the beam as well as the coupling conditions to consider the pressure loading on each side of the beam in typical vibroacoustic problems. It can be observed that $\varphi_r(2^j\eta_m - n)$ is generated from one single function $\varphi_r(\eta_m)$ by using particular scale and translation values. The approximation resolution of the enrichment functions is controlled by the scale and the hierarchic refinement can be implemented by adjusting the value of j [35]. Better resolutions can be obtained by using enrichment functions with a larger scaling parameter j or a shorter support length, as shown in Figs. 3 (a) and (b). The wavelet enrichment should be applied with an ordinary mesh and a sufficient high resolution [34, 38, 18]. To avoid the singularity in the numerical calculation, the range of n should be truncated and selected so that the wavelet enrichment functions have non-zero values within the bounded interval of η_m, which is illustrated in Fig. 3 (a). The advantage of using B-spline wavelets is that its scaling functions are analytically expressible, thus conducive to numerical implementation [35]. Meanwhile, B-spline scaling function exhibits smooth oscillations within its support than other types of wavelets, like Daubechies wavelet [38]. As a result, the resultant system matrix is better conditioned and can be evaluated with much reduced Gauss points. A systematic hierarchic refinement can then be conducted without much numerical difficulties. The quintic B-spline function φ_6 [39] is chosen as wavelet enrichment in this work to show that the wavelet enrichment can improve the computational performance of the PUFEM when applied to ABH vibration problems, rather than focusing on comparisons among different types of wavelets.

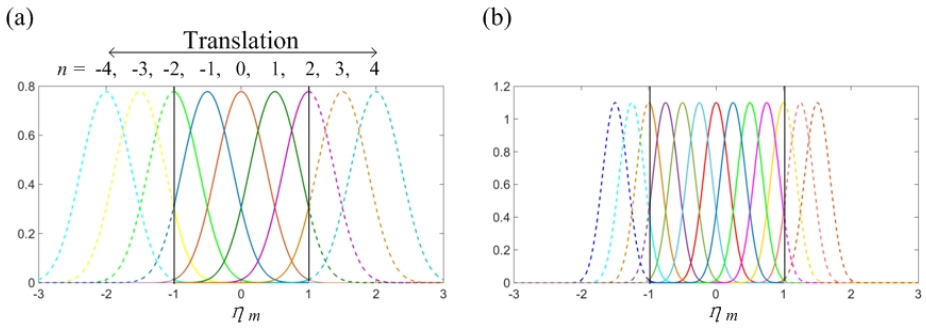

Figure 3: (a) Quintic spline scaling functions with $j = 1$ and (b) quintic spline scaling functions with $j = 2$.

3. Numerical Analyses and Discussions

A quadratic wedge-like ABH beam with a variable rectangular cross section is taken as the test configuration in this section (Fig. 1 (a)). Geometrical and material parameters of the tested ABH wedge are given in Table 1. Both ends of the beam are free of constraints. A unit harmonic point loading is imposed at the right end $x_f = L$ to activate the ABH taper, corresponding to a node of the mesh.

Wedge thickness	$h(x) = 0.01(x + 0.02)^2/(0.2 + 0.02)^2,\ 0 \leq x \leq L$
Length and width	$L = 0.2$ m, $t = 0.01$ m
Material properties	$E = 70$ GPa, $G = 27$ GPa, $\rho = 2780$ kg/m^3

Table 1: Geometrical and material parameters used in our computations.

3.1. PUFEM computational performance

The performance of PUFEM with different enrichment functions is first investigated. To this end, cross Frequency Response Functions (FRF) are calculated and compared with the reference solution obtained from the classical linear FEM, as shown in Fig. 4. The point response is evaluated at $0.3L$ from the left end of the beam ($x = 0.06$m). The reference FEM solution is obtained using 10,000 classical Timoshenko beam elements with linear shape functions and the reduced Gauss integration scheme is adopted for calculating the stiffness matrix to avoid shear locking [33, 18]. The FRF curves of the PUFEM with WKB wave enrichment and local wave enrichment are calculated with 16 elements of equal length and 5 enrichment functions. The corresponding number of DoFs is $17 \times 5 \times 2 = 170$. The calculation of the wavelet enrichment is carried out with 4 elements of same length. The scaling parameter j is set to be 3 so that the total number of DoFs, here 188, is comparable with that of the wave enrichment.

Comparative results using the WKB wave enrichment are given in Figs. 4 (a) and (b). It can be seen that the structure under investigation exhibits rather complex dynamics, evidenced by multiple structural resonances. Generally speaking, a good agreement between the WKB wave-enriched elements and the reference solution can be observed within the entire frequency band. Therefore, the WKB Euler-Bernoulli and Timoshenko enrichment provide similar performance in terms of accuracy. The point response of the enrichment using analytical Euler-Bernoulli solutions is similar to that based on WKB solutions, which is not shown here for simplicity.

Two other types of enrichment, using wavelet and local wave functions, are also compared with reference FEM solution in Figs. 4 (c) and (d), respectively. It can be seen that both can

offer accurate predictions up to a certain frequency limit, above which the PUFEM curves start to deviate from the reference solution. More specifically, the wavelet enrichment (Figs. 4 (d)) can ensure the accuracy up to around 23 kHz, outperforming the local wave enrichment, which can roughly reach 10 kHz with reasonably good accuracy. It should be stressed that the above comparisons involve formulations with roughly the same number of DoFs. As will be illustrated later by convergence studies, the working frequency band of the PUFEM can be extended by using mesh refinement or by increasing the wavelet resolution.

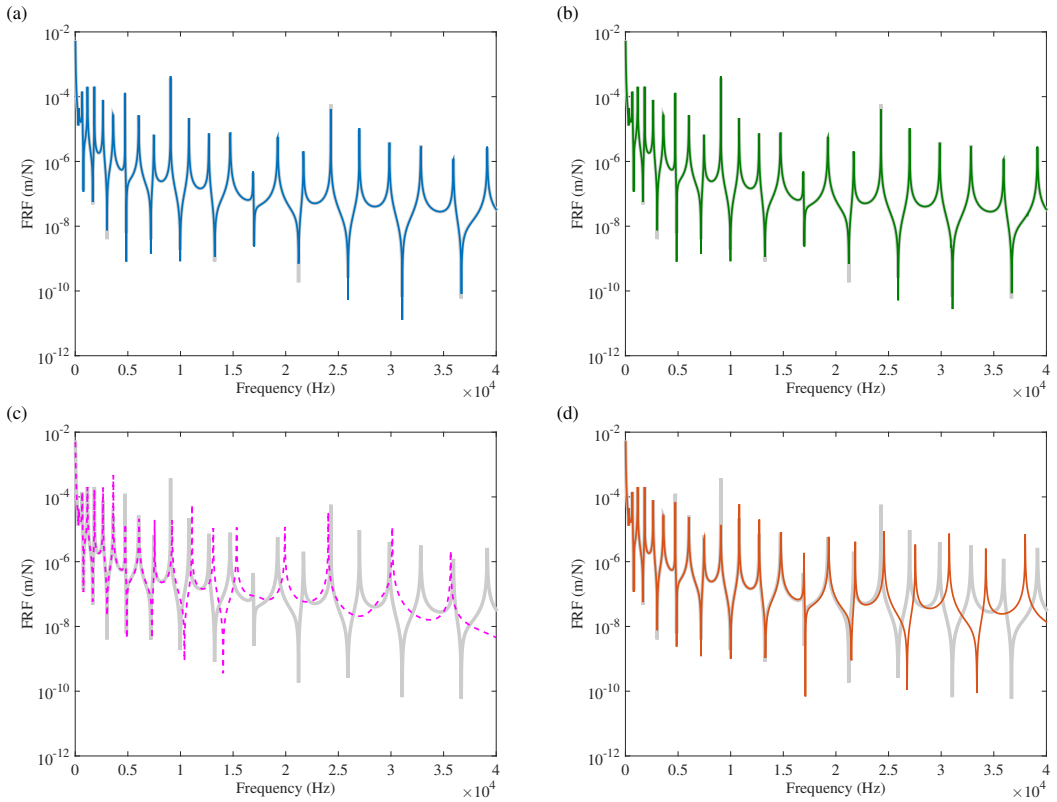

Figure 4: FRF curves w/F_0 (at $0.3L$ from left end) calculated by the PUFEM with: (a) —— WKB Euler-Bernoulli enrichment, (b) —— WKB Timoshenko enrichment, (c) - - - local wave enrichment, (d) —— wavelet enrichment. —— reference solution with classical FEM.

To examine the ability of the PUFEM in characterizing typical ABH-specific features, Figs. 5 (a)-(c) show the structural response along the ABH wedge near the upper working frequency range in Fig. 4 using different enrichment methods. Results from the classical linear FEM with 100 elements (202 DoFs) are also shown in Fig. 5 (d) for comparison purposes. One can observe the typical ABH phenomena from plotted deformation shapes: gradually shortened local wavelengths and increased oscillating amplitudes along the reduced structural thickness. Comparisons in Fig. 5 also illustrate that, by using the similar number of DoFs, the element enriched with WKB wave functions can cope with more spatial oscillations than other types of elements. Meanwhile, the wavelet enrichment can also provide a good approximation over the whole problem domain. On the contrary, the enrichment with the local wave solution, whose wavenumber is evaluated at each node and holds a constant value over the element (Eq. (18)), shows less accurate results in terms of depicting the strong variation of wavenumbers and amplitudes within the element at higher frequencies. It is also found that all PUFEM elements perform better than

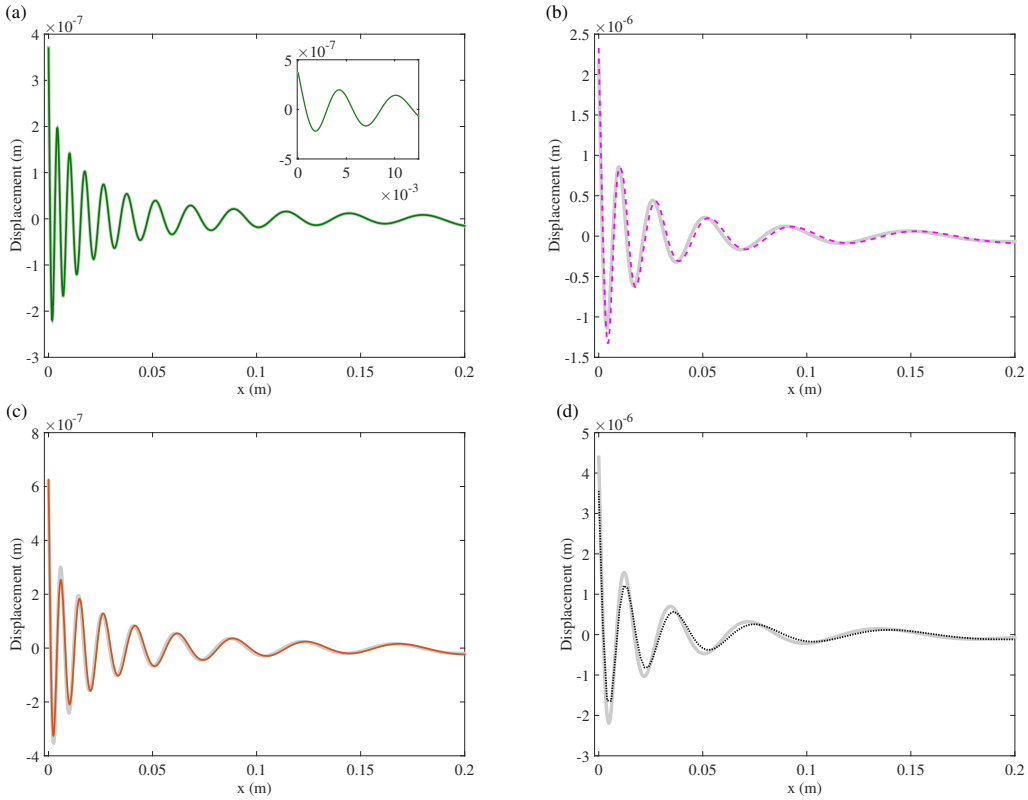

Figure 5: The deformed shapes along the ABH wedge calculated by the PUFEM with (a) —— WKB Timoshenko enrichment at 40 kHz, (b) – – – local wave enrichment at 10 kHz , (c) —— wavelet enrichment at 23 kHz, and by (d) ------- the linear FEM (100 elements) at 7 kHz. —— the corresponding reference solution with classical FEM.

the linear FEM (Fig. 5 (d)). Deviations and mismatch of calculated shapes with the reference solution at the thin wedge part can be observed for the PUFEM with wavelet and local wave functions and the linear FEM. The zoom-in sub-figure in Fig. 5 (a) shows the detailed structural displacement within the 1st element from the left end (thin part of the ABH wedge). One can observe that a single enriched element can capture multiple wavelengths (more than 2 for the present case), which is a typical feature of wave enrichment, as well as the ABH-induced wave modulation effects.

Figure 6 presents the comparison of the convergence of different formulations at two selected frequencies, 20 kHz and 40 kHz. In the present case, the wedge is meshed by the elements with equal length. All convergence curves, except for the PUFEM with wavelet enrichment, are obtained by using the mesh refinement, i.e. reducing element spacing from a coarse mesh. The wavelet enrichment is refined by increasing the scaling parameter j, with the element number kept at 4. The L^2 errors are plotted against the number of DoFs. The relative errors are estimated via L^2-norm as

$$\varepsilon = \frac{\sqrt{\int_0^L |w_{computed} - w_{ref}|^2 \mathrm{d}x}}{\sqrt{\int_0^L |w_{ref}|^2 \mathrm{d}x}} \times 100\% \,, \tag{20}$$

where w_{ref} is the reference solution. The reference FEM solution for convergence studies is obtained by using 200,000 elements with linear shape functions and reduced Gauss integration. According to Fig. 6, the PUFEM with WKB Euler-Bernoulli and Timoshenko enrichment and

the analytical Euler-Bernoulli enrichment all converge to the reference solution faster than the other formulations and can achieve reasonably good accuracy with a relatively small number of DoFs. Typically, the errors of all these wave-enriched elements drop below 1% when the DoF number is larger than 80 and reach $10^{-4}\%$ level when further increased to 500. It should be noted that the error estimation here is limited by the resolution of the reference solution, which explains the sudden change of the curve shape around a very low error percentage $O(10^{-4})$. The difference in terms of convergence between the PUFEM elements, enriched with WKB approximate solutions and with the analytical wave solution, is not significant. At the higher frequency of 40 kHz, the advantage of the analytical wave enrichment becomes less obvious and the WKB Timoshenko enrichment works slightly better than WKB Euler-Bernoulli enrichment. Note that a quadratic wedge is taken as the tested configuration in this work so that analytical wave enrichment functions exist, while the WKB approximation can be used for tapered wedge with general profiles. Therefore, the WKB methods can provide good approximation functions for the PUFEM tapered Timoshenko beam element. It can also be found from Fig. 6 that the wavelet-enriched elements and those by local wave functions have higher convergence rates than the classical linear element and can reach high accuracy with a much smaller number of DoFs. The convergence results indicate their relative errors behaving like $\varepsilon \sim \mu\, {l_e}^{\tau}$ in which $\tau \approx 7$ (l_e is the element length and is inversely proportional to the total number of DoFs). Compared with the local wave enrichment, the wavelet enrichment has smaller values for the constant μ and thus better computational efficiency. The results show that all types of PUFEM formulations outperform classical linear FEM and the classical linear element has the expected convergence rate of 2.

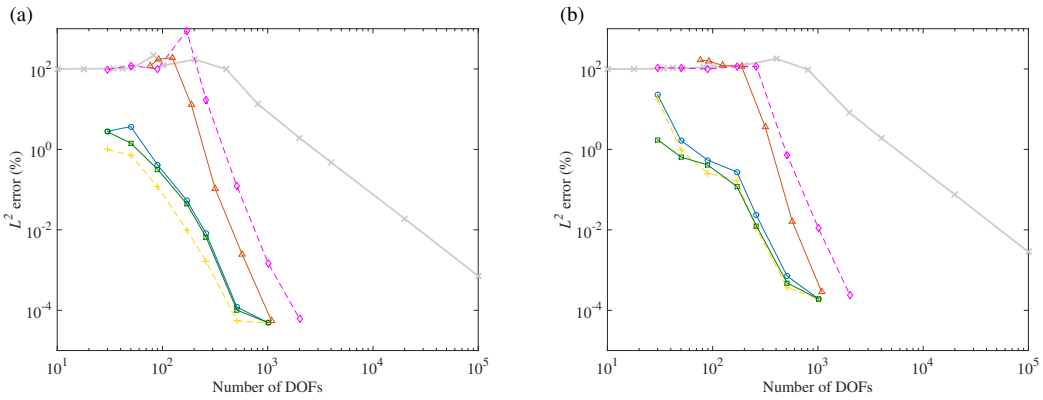

Figure 6: Comparison of convergence at (a) 20 kHz and (b) 40 kHz. classical linear FEM, PUFEM with WKB Euler-Bernoulli enrichment, PUFEM with WKB Timoshenko enrichment, PUFEM with analytical Euler-Bernoulli enrichment, PUFEM with wavelet enrichment, PUFEM with local wave enrichment.

3.2. PUFEM with adaptive mesh

To reduce the calculation errors and enhance the convergence of the numerical solutions, an adaptive mesh scheme is proposed and implemented for the formulations discussed previously. The mesh design is based on the characteristics of wave propagation in an ABH wedge.

According to Eq. (5), the local wavenumber $\bar{k}(x)$ is inversely proportional to the square root of the local thickness $\sqrt{h(x)}$, so the local wavelength in the quadratic ABH taper will increase linearly along x-coordinate. In the proposed discretization scheme, the mesh spacing is

therefore adapted with a linear increase along the wedge length coordinate and the difference in lengths between the two neighbouring elements is set to be constant. This non-uniform mesh allows a finer resolution at the thin portion of the wedge, where the wave amplitude undergoes severer variations. Carrying out the same refinement used in Fig. 6, Fig. 7 shows the comparison between the convergence curves of the PUFEM with WKB Timoshenko enrichment and wavelet enrichment using uniform mesh and adaptive mesh, at two selected frequencies, respectively. It can be seen that the non-uniform adaptive mesh can effectively reduce the numerical error for all enrichments. More specifically, with the number of DoFs above 150, the adaptive mesh reduces the error by roughly two orders of magnitude as compared to the uniform mesh. Comparing different formulations using adaptive mesh (results not shown here), it was observed that conclusions obtained from the uniform mesh still apply: the wave enrichment based on the WKB and analytical solutions shows the best performance and the wavelet enrichment outperforms the local wave enrichment and the classical linear element. Figure 8 compares the convergence properties among various wave enrichment with different solutions using adaptive mesh at 40 kHz. It can be observed that the WKB Timoshenko enrichment shows superiority over both WKB and analytical Euler-Bernoulli enrichment at 40 kHz when using the adaptive mesh refinement, suggesting a greater contribution of the shear and rotation inertia effects.

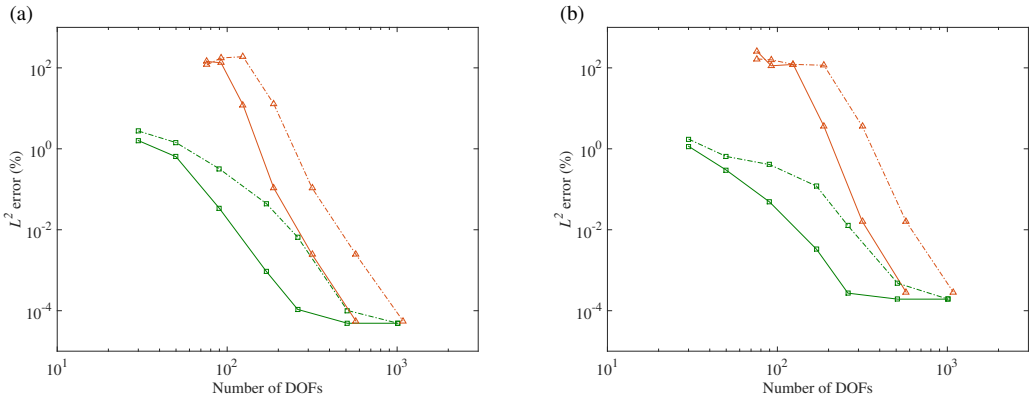

Figure 7: Comparison of convergence at (a) 20 kHz and (b) 40 kHz. WKB Timoshenko enrichment using uniform mesh, WKB Timoshenko enrichment using adaptive mesh, wavelet enrichment using uniform mesh, wavelet enrichment using adaptive mesh.

3.3. Applicability of WKB approach

As mentioned above, the applicability of the WKB approximation method relies on the condition of sufficient smoothness of the beam thickness variation: the change in the local wavenumbers along the tapered beam should be small over a distance comparable to one wavelength. The NWV, i.e. the left-hand side term of Eq. (7), provides an estimation of the validity of the WKB method. For a given quadratic Euler-Bernoulli wedge, NWV is only dependent on the frequency but not the position [1]. Therefore, at higher frequencies, the NWV is smaller and the WKB approximation is more accurate. It is opined that, in the low frequency range, the NWV should be kept below 0.3 to satisfy the sufficient smoothness condition [7]. Previous works on the validity of the WKB method for ABH problems were conducted based on the reflection coefficients of propagating waves [40, 7]. The applicability of the WKB method under the PUFEM framework can be evaluated in terms of vibrational response using the element enriched with WKB wave functions. Results suggest that the WKB approach can still provide

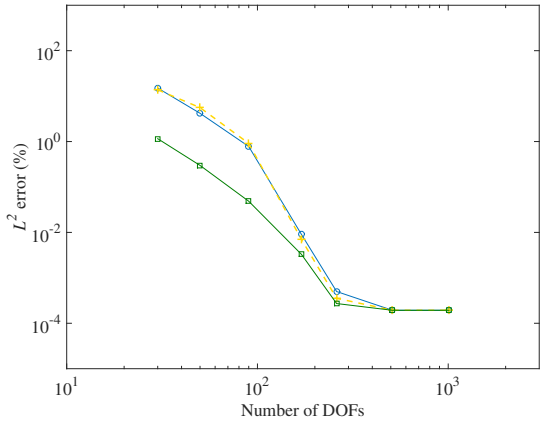

Figure 8: Convergence curves of wave enrichment at 40 kHz using adaptive mesh —○— WKB Euler-Bernoulli enrichment, —□— WKB Timoshenko enrichment, – + – analytical Euler-Bernoulli enrichment,

appropriate approximation functions with good accuracy for the PUFEM in the low frequency range even with NWV values which are considered to be high from the view point of wave reflection. For the test case used in the present study, the NWV value is 0.4 at 300 Hz, which is between the 1st and 2nd resonance frequencies of the beam. By using one single element, the relative error using the element enriched with WKB Euler-Bernoulli or Timoshenko solutions is around 0.01% while the one with analytical Euler-Bernoulli enrichment is near $10^{-4}\%$. At other low frequencies with a large NWV, similar observations can be made using a small number of elements: the WKB wave-enriched elements can provide reasonably accurate results, albeit not as accurate as the analytical Euler-Bernoulli enrichment.

4. Conclusions

In this work, the PUFEM tapered Timoshenko beam elements are developed to solve the forced vibration response of an ABH wedge. Several types of PUFEM elements are constructed using different enrichment functions, namely wave enrichment based on WKB approximate solutions for the tapered Euler-Bernoulli and Timoshenko beams and the one based on wavelets. The computational performance of different formulations is evaluated in terms of structural response and solution convergence. By capitalizing on the ABH-specific wavelength variation, an adaptive mesh scheme is also proposed.

The prevailing conclusions are given below:

1). Through numerical simulations and analyses, it was shown that, upon a proper selection of the enrichment scheme, the PUFEM is capable of predicting and reproducing the typical ABH-induced wave phenomena in a broad frequency band, by using a relatively small number of DoFs. This reduction of DoFs is achieved by the enrichment enabling one single element to capture multiple wavelengths and local wavelength variation.

2). The performance of the PUFEM shows strong dependence on the matching between the approximation properties of the enrichment functions and the physical nature of the ABH phenomena. The WKB wave enrichment, crafted with the inherent wave propagation information of the tapered beam, offers the best performance in terms of computational accuracy and data reduction. The wavelet enrichment functions can also provide an efficient and accurate approximation for the ABH-induced wave behaviour. The wavelet-enriched element shows its

versatility and flexibility in dealing with the strongly localized and highly oscillatory system behaviour owing to its compact support, flexible scaling and translation features.

3). The PUFEM with the WKB wave solutions and the wavelet functions show superiority over the enrichment with the nodal-defined local wave solutions and the classical linear FEM. The proposed adaptive mesh scheme is shown to further increase the computational efficiency of the PUFEM.

4). Through comparisons with analytical wave enrichment, the WKB wave solutions are found to be good approximation functions for PUFEM, applicable at relatively low frequencies where the sufficient smoothness hypothesis may not be strictly satisfied.

As a final remark, an overall strategy based on different PUFEM formulations has been established for solving the structural vibration problem of an ABH tapered wedge. The PUFEM allows easy inter-element connections. In a broader perspective, the proposed PUFEM framework can also be applied to other beams with a thickness variation going beyond the scope of ABH beams, and eventually be extended to other physical problems with spatially varying wave speeds. Future effort is needed to apply the present numerical approach for solving more practical problems, such as ABH wedges with surface damping treatment or vibroacoustic coupling systems.

5. Acknowledgements

The authors thank the support from Research Grant Council of the Hong Kong SAR (PolyU 152017/17E) and National Science Foundation of China (No. 11532006).

6. References

[1] M.A. Mironov. Propagation of a flexural wave in a plate whose thickness decreases smoothly to zero in a finite interval. *Soviet Physics Acoustics-USSR*, 34(3):318–319, 1988.

[2] V.V. Krylov and F.J.B.S. Tilman. Acoustic black holes for flexural waves as effective vibration dampers. *Journal of Sound and Vibration*, 274(3-5):605–619, 2004.

[3] V. Denis, A. Pelat, F. Gautier, and B. Elie. Modal overlap factor of a beam with an acoustic black hole termination. *Journal of Sound and Vibration*, 333(12):2475–2488, 2014.

[4] V.B. Georgiev, J. Cuenca, F. Gautier, L. Simon, and V.V. Krylov. Damping of structural vibrations in beams and elliptical plates using the acoustic black hole effect. *Journal of Sound and Vibration*, 330(11):2497–2508, 2011.

[5] X. Li and Q. Ding. Analysis on vibration energy concentration of the one-dimensional wedge-shaped acoustic black hole structure. *Journal of Intelligent Material Systems and Structures*, 29(10):2137–2148, 2018.

[6] L. Tang, L. Cheng, H. Ji, and J. Qiu. Characterization of acoustic black hole effect using a one-dimensional fully-coupled and wavelet-decomposed semi-analytical model. *Journal of Sound and Vibration*, 374:172–184, 2016.

[7] P.A. Feurtado and S.C. Conlon. Investigation of boundary-taper reflection for acoustic black hole design. *Noise Control Engineering Journal*, 63(5):460–466, 2015.

[8] T. Zhou, L. Tang, H. Ji, J. Qiu, and L. Cheng. Dynamic and static properties of double-layered compound acoustic black hole structures. *International Journal of Applied Mechanics*, 9(05):1750074, 2017.

[9] L. Tang and L. Cheng. Broadband locally resonant band gaps in periodic beam structures with embedded acoustic black holes. *Journal of Applied Physics*, 121(19):194901, 2017.

[10] T. Zhou and L. Cheng. A resonant beam damper tailored with acoustic black hole features for broadband vibration reduction. *Journal of Sound and Vibration*, 430:174–184, 2018.

[11] M.R. Shepherd, P.A. Feurtado, and S.C. Conlon. Multi-objective optimization of acoustic black hole vibration absorbers. *The Journal of the Acoustical Society of America*, 140(3):EL227–EL230, 2016.

[12] C. McCormick and M. Shepherd. Optimal design and position of an embedded one-dimensional acoustic black hole. In *INTER-NOISE and NOISE-CON Congress and Conference Proceedings*, volume 258, pages 1345–1354. Institute of Noise Control Engineering, 2018.

[13] J.M. Melenk and I. Babuška. The partition of unity finite element method: Basic theory and applications. *Computer Methods in Applied Mechanics and Engineering*, 139:289–314, 1996.

[14] I. Babuska and J.M. Melenk. The partition of unity method. *International Journal for Numerical Methods in Engineering*, 40(4):727–758, 1997.

[15] O. Laghrouche and M.S. Mohamed. Locally enriched finite elements for the helmholtz equation in two dimensions. *Computers and Structures*, 88:1469–1473, 2010.

[16] M. Yang, E. Perrey-Debain, B. Nennig, and J.-D. Chazot. Development of 3d pufem with linear tetrahedral elements for the simulation of acoustic waves in enclosed cavities. *Computer Methods in Applied Mechanics and Engineering*, 335:403 – 418, 2018.

[17] A. El Kacimi and O. Laghrouche. Numerical modelling of elastic wave scattering in frequency domain by the partition of unity finite element method. *International Journal for Numerical Methods in Engineering*, 77(12):1646–1669, 2009.

[18] T. Zhou, J.-D. Chazot, E. Perrey-Debain, and L. Cheng. Performance of the partition of unity finite element method for the modeling of timoshenko beams. *Computers & Structures*, 222:148–154, 2019.

[19] O. Laghrouche, P. Bettess, E. Perrey-Debain, and J. Trevelyan. Wave interpolation finite elements for helmholtz problems with jumps in the wave speed. *Computer Methods in Applied Mechanics and Engineering*, 194:367–381, 2005.

[20] J.-D. Chazot, B. Nennig, and E. Perrey-Debain. Performances of the partition of unity finite element method for the analysis of two-dimensional interior sound fields with absorbing materials. *Journal of Sound and Vibration*, 332(8):1918–1929, 2013.

[21] J.-D. Chazot, E. Perrey-Debain, and B. Nennig. The partition of unity finite element method for the simulation of waves in air and poroelastic media. *Journal of the Acoustical Society of America*, 135(2):724–733, 2014.

[22] R.J. Astley and P. Gamallo. Special short wave elements for flow acoustics. *Computer Methods in Applied Mechanics and Engineering*, 194(2-5):341–353, 2005.

[23] P. Gamallo and R.J. Astley. The partition of unity finite element method for short wave acoustic propagation on non-uniform potential flows. *International Journal for Numerical Methods in Engineering*, 65(3):425–444, 2006.

[24] P. Ortiz. Finite elements using a plane-wave basis for scattering of surface water waves. *Philosophical Transactions of the Royal Society of London. Series A: Mathematical, Physical and Engineering Sciences*, 362(1816):525–540, 2004.

[25] P. Bettess. Special wave basis finite elements for very short wave refraction and scattering problems. *Communications in numerical methods in engineering*, 20(4):291–298, 2004.

[26] L. M. Imbert-Gérard and B. Després. A generalized plane-wave numerical method for smooth nonconstant coefficients. *IMA Journal of Numerical Analysis*, 34(3):1072–1103, 2013.

[27] A.W. Leissa and M.S. Qatu. *Vibrations of Continuous Systems.* McGraw-Hill, 2011.

[28] M.H. Holmes. *Introduction to perturbation methods*, volume 20. Springer Science & Business Media, 2012.

[29] A.D. Pierce. Physical interpretation of the wkb or eikonal approximation for waves and vibrations in inhomogeneous beams and plates. *The journal of the Acoustical Society of America*, 48(1B):275–284, 1970.

[30] V.V. Krylov. Conditions for validity of the geometrical-acoustics approximation in application to waves in an acute-angle solid wedge. 1989.

[31] V.V. Krylov. Geometrical-acoustics approach to the description of localized vibrational modes of an elastic solid wedge. 1990.

[32] M.A. Mironov. Exact solutions of equation of transverse vibrations for a bar with a specific cross section variation law. *Acoustical Physics*, 63(1):1–6, 2017.

[33] M. Petyt. *Introduction to finite element vibration analysis*. Cambridge university press, 2010.

[34] C.K. Chui. *An introduction to wavelets*. Boston: Academic Press, 1992.

[35] K. Urban. *Wavelet methods for elliptic partial differential equations*. Oxford University Press, 2009.

[36] L. Ma, S. Zhang, and L. Cheng. A 2d daubechies wavelet model on the vibration of rectangular plates containing strip indentations with a parabolic thickness profile. *Journal of Sound and Vibration*, 429:130–146, 2018.

[37] A. Katunin and A. Korczak. The possibility of application of b-spline family wavelets in diagnostic signal processing. *acta mechanica et automatica*, 3:43–48, 2009.

[38] S. Zhang and L. Cheng. On the efficacy of the wavelet decomposition for high frequency vibration analyses. *Journal of Sound and Vibration*, 380:213–223, 2016.

[39] G.V. Milovanović and Z. Udovičić. Calculation of coefficients of a cardinal b-spline. *Applied Mathematics Letters*, 23(11):1346–1350, 2010.

[40] V. Denis, F. Gautier, A. Pelat, and J. Poittevin. Measurement and modelling of the reflection coefficient of an acoustic black hole termination. *Journal of Sound and Vibration*, 349:67–79, 2015.